Accepted for publication in Building and Environment

High-resolution CFD simulations for forced convective heat transfer coefficients at the facade of a low-rise building

B. Blocken* [(a)], T. Defraeye [(b)], D. Derome [(c)], J. Carmeliet [(d,e)]

(a) Building Physics and Systems, Eindhoven University of Technology, P.O. box 513, 5600 MB Eindhoven, The Netherlands
(b) Laboratory of Building Physics, Katholieke Universiteit Leuven, Kasteelpark Arenberg 40, 3001 Leuven, Belgium
(c) Wood Laboratory, Empa, Swiss Federal Laboratories for Materials Testing and Research, Überlandstrasse 129, CH-8600 Dübendorf, Switzerland
(d) Chair of Building Physics, Swiss Federal Institute of Technology ETHZ, ETH-Hönggerberg, CH-8093 Zürich, Switzerland
(e) Laboratory for Building Technologies, Empa, Swiss Federal Laboratories for Materials Testing and Research, Überlandstrasse 129, CH-8600 Dübendorf, Switzerland

Abstract

High-resolution 3D steady RANS CFD simulations of forced convective heat transfer at the facades of a low-rise cubic (10x10x10 m³) building are performed to determine convective heat transfer coefficients (CHTC). The focus is on the windward facade. CFD validation is performed based on wind tunnel measurements of velocity and heat transfer for reduced-scale cubic models. The CFD simulations employ a high-resolution grid with, for the 10 m cubic building, cell centres at a minimum distance of 160 μm from the building surface to resolve the entire boundary layer, including the viscous sublayer and the buffer layer, which dominate the convective surface resistance. The results show that: (1) the wind flow around the building results in highly varying CHTC values across the windward facade; (2) standard and non-equilibrium wall functions are not suitable for CHTC calculation, necessitating either low-Reynolds number modelling or specially-adapted wall functions; (3) at every facade position, the CHTC is a power-law function of the mean wind speed; (4) the CHTC distribution at the windward facade is relatively insensitive to wind direction variations in the 0º to 67.5º angle range; (5) the CHTC shows a stronger spatial correlation with the turbulent kinetic energy than with the mean wind speed across the facade; (6) the CHTC distribution across the windward facade is quite similar to the distribution of wind-driven rain (WDR), with both parameters reaching high levels near the top edge of the facade. This suggests that also the convective moisture transfer coefficient will be higher at this location and that the facade parts that receive most WDR might also experience a higher drying rate.

Keywords: Surface coefficients; Heat, air, moisture transfer (HAM); Mass transfer; Computational Fluid Dynamics (CFD); Building Envelope; Urban climatology

1. Introduction

Hygrothermal analysis of building components, which includes heat, air and moisture transport (HAM), requires the knowledge of the convective heat transfer coefficient (CHTC) and the convective moisture transfer coefficient (CMTC) at exterior and interior building surfaces:

$$h_c = \frac{q_c}{(T_s - T_{ref})} \quad (1)$$

* Corresponding author: Bert Blocken, Building Physics and Systems, Eindhoven University of Technology, P.O. box 513, 5600 MB Eindhoven, the Netherlands. Tel: +31 (0)40 247 2138, Fax: +31 (0)40 243 8595. *E-mail address:* b.j.e.blocken@tue.nl

$$h_m = \frac{g_v}{(p_{v,s} - p_{v,ref})} \quad (2)$$

where h_c is the CHTC (W/m²K), q_c the convective heat flux density (W/m²), T_s the surface temperature (K) and T_{ref} the reference temperature (K), h_m is the CMTC (s/m), g_v the convective vapour flux density (kg/m²s), $p_{v,s}$ the vapour pressure at the surface (Pa) and $p_{v,ref}$ the reference vapour pressure (Pa). Past as well as very recent research on CHTC and CMTC for building applications has mostly focused on interior building surfaces [e.g., 1]. Less attention has been given to the study of transfer coefficients at exterior surfaces. Knowledge of the exterior CHTC is important for investigating the thermal performance of single-glazed historical buildings, double-skin facades, green houses, tent-like structures, solar collectors, solar chimneys, ventilated photovoltaic arrays, etc. Information on the exterior CHTC and CMTC is required for the analysis of wetting and drying of building components and the related damage processes. Both parameters are also needed for larger-scale urban climatology studies. Determining the values of exterior transfer coefficients across building facades is a difficult task, because they are a complex function of a wide range of parameters including building geometry, environment topography, wind speed, wind direction, turbulence intensity, surface roughness, texture and geometry, and moisture content. The present paper focuses on exterior CHTC only. Note that values of exterior CMTC for HAM modelling are usually obtained from the CHTC by assuming the Chilton-Colburn analogy [2], although previous studies have shown this to be incorrect for porous building materials [3-5].

In the past, three methods have been employed to investigate and determine exterior CHTC for building applications: wind tunnel measurements, full-scale measurements and numerical simulations with Computational Fluid Dynamics (CFD). Most research up to now has been experimental. A brief, non-exhaustive overview is provided below.

Jürges [6] performed a wind tunnel study of the convective heat transfer from small, flat, heated plates attached to the wall of a wind tunnel. For a smooth surface, the following relationship of h_c with the free-stream wind speed in the tunnel V_∞ was obtained:

$$h_c = 4.0 V_\infty + 5.6 \quad ; \quad V_\infty < 5 \text{ m/s} \quad (3)$$

$$h_c = 7.1 V_\infty^{0.78} \quad ; \quad V_\infty > 5 \text{ m/s} \quad (4)$$

Although the flow in these tests did not resemble the complex flow pattern around a building, these results were used as the basis of the design values of h_c as for example given in the 1979 CIBS Guide [7]. Although the influence of wind speed is important, as indicated by Eqs. (3-4), this version of the Guide did not provide sufficient information on local wind speed. Actually, V_∞ in Eqs. (3-4) seems to have been replaced by a local wind speed $V_{3D,loc}$ near the building surface, although both parameters can be considerably different. The local wind speed $V_{3D,loc}$ is defined as the magnitude of the 3D velocity vector, taken at a certain distance d from the facade. Furthermore, the Guide assumed that $V_{3D,loc}$ does not vary across the facade and did not specify at what facade location and at what distance from the facade this value has to be taken.

From the mid 1960's, several attempts were made to measure h_c with heated plates or strips on full-scale buildings. In 1972, Ito et al. [8] reported measurements of h_c and $V_{3D,loc}$ (at 0.3 m distance from the heated surface) at eight different positions at the facade of a 6-storey building in Tokyo, and the wind speed V_R at 8 m above the roof. The conclusions from this work were: (1) For the windward surface, $V_{3D,loc}$ is about 0.20-0.33 times V_R, and a general relationship between $V_{3D,loc}$ and V_R is difficult to establish; (2) The h_c-$V_{3D,loc}$ relationship is relatively independent of location on the surface and wind direction; (3) The relationship between V_R and h_c can be broken down into two characteristic relationships: the relationship between V_R and $V_{3D,loc}$, which is dependent on the location on the surface and the wind direction, and the relationship between $V_{3D,loc}$ and h_c, which is relatively independent of the location on the surface and the wind direction. However, these conclusions were based on results from a limited number of positions on the facade and for a small range of wind directions. The wind directions for windward exposure were all nearly perpendicular to the test facade. The work by Ito et al. was the basis for the empirical relationships between U_{10}, $V_{3D,loc}$ and h_c, set forth by the ASHRAE Task Group in 1975 [9]. U_{10} is defined as the reference wind speed at 10 m height. Unfortunately, V_R in the equations of Ito et al. appears to have been substituted by U_{10}, while it had been shown that the difference between U_{10} and V_R can be quite large in the complex wind-flow pattern around buildings [10-12].

In 1984, Sharples [13] reported his measurements of the forced h_c and $V_{3D,loc}$ (at 1 m from the surface) at four different facade positions and V_R at 6 m above the roof of a high-rise building (18 storeys; 78 m), as well as U_{10} at a nearby meteorological station. As opposed to the findings by Ito et al. [8], the h_c-$V_{3D,loc}$ relationship did not appear to be independent of the location on the surface and the wind direction. Sharples [13] attributed this different result to the small range of wind speeds and wind directions in the study by Ito et al. For a "worse case" situation, i.e. a location at the top edge of the 18-storey high-rise building, Sharples [13] presented the following relationship:

$$h_c = 1.7\,V_{3D,loc} + 5.1 \quad (W/m^2K) \tag{5}$$

where $V_{3D,loc}$ is the local wind speed (m/s) measured at 1 m distance from the surface. It can be expressed as a function of the reference wind speed U_{10} (m/s) [13]:

$$V_{3D,loc} = 1.8\,U_{10} + 0.2 \quad (m/s)\ (windward) \tag{6}$$

$$V_{3D,loc} = 0.2\,U_{10} + 1.7 \quad (m/s)\ (leeward) \tag{7}$$

Note that Sharples [13] adopted a rather coarse classification of wind direction with only two classes; windward and leeward: "*data was classified as windward if the angle of incidence between the normal to the monitored facade and the wind direction, θ, was less than +/-90° and leeward for all other directions*".

Loveday and Taki [14] measured h_c at a plane, smooth test panel, fixed at the centre of the 6th floor facade of an 8-storey (28 m) building. The facade was characterised as relatively flat and undisrupted. Correlations were established between h_c and $V_{3D,loc}$ measured at 1 m from the surface and V_R at 11 m above the roof. These authors indicated that more care is needed in classifying facades according to wind direction, because flow that is nearly parallel to a windward facade can lead to leeward-like CHTC values due to flow separation. They also clearly pointed out the conditions for which their correlations can be used. More recently, Liu and Harris [15] measured h_c at the facade of a low-rise (5.6 m high) building in sheltered conditions and correlated it with $V_{3D,loc}$ at 0.5 m from the surface, V_R at 1m above the roof, and U_{10}. Also these authors pointed to the too coarse traditional "windward-leeward" classification.

CFD simulations of the exterior CHTC on the surfaces of a rectangular, low-rise building model (L x B x H = 8 x 6 x 2.7 m³) were performed by Emmel et al. [16] using the Reynolds-averaged Navier Stokes (RANS) equations. However, the coarse grid near the building surfaces and the use of wall functions have compromised the accuracy of these calculations, because the most important parts of the boundary layer, the viscous sublayer and the buffer layer, which dominate the convective surface resistance, were not resolved. The errors that are introduced by this approach will be demonstrated later in this paper.

The existing empirical formulae for the CHTC as a function of wind speed are based on only a limited number of measurements for a few building configurations and at a few facade positions. As more detailed information is not available, most state-of-the-art HAM models, e.g., [17], generally use Eqs. (5-7) for all types of buildings and at all facade positions. Even if the building in the HAM analysis would be identical to the building in the analysis of Sharples [13], these equations can provide a severe overestimation of the CTHC at most facade positions, because Eqs. (5-7) only hold for the top edge of a 78 m high building.

Therefore, a more complete understanding of convective heat and mass transfer is needed to provide better CHTC and CMTC values for HAM modelling. The same three options as mentioned above are available: wind tunnel measurements, full-scale measurements and CFD simulations. Wind tunnel measurements can suffer from incompatible similarity requirements and obtaining high-resolution spatial information requires measurement techniques such as infrared thermography. Full-scale measurements are expensive and time-consuming, and generally only provide information at a few selected locations at the facade. CFD can provide a suitable alternative, but the accuracy of CFD is an important matter of concern and careful application, validation and verification are imperative.

This paper presents high-resolution 3D CFD simulations of forced convective heat transfer at the facades of a low-rise cubic building (10 x 10 x 10 m³) to determine convective heat transfer coefficients (CHTC). Forced convection implies that buoyancy forces arising from density changes are not included. The focus is on the windward facade. The objectives are: (1) to determine the distribution of the CHTC across the facade; (2) to assess the impact of low-Reynolds number modelling versus wall-function modelling on the accuracy of CTHC simulations; (3) to analyse the variation of the CHTC with wind

speed; and (4) of the CHTC with wind direction; (5) to analyse the relationship between h_c and $V_{3D,loc}$ taken at different positions from the facade and across the facade; and (6) to briefly address the relationship between CHTC and wind-driven rain (WDR) distributions at the windward facade.

In section 2, the two main approaches for near-wall modelling are briefly outlined. In section 3, CFD validation is performed. Section 4 describes the application of the validated model for forced convective heat transfer at the exterior surfaces of the cubic building. The results are reported in section 5. Sections 6 and 7 present a discussion and the conclusions.

2. Low-Reynolds number modelling versus wall functions

In CFD simulations, generally, two options for modelling flow parameters in the near-wall region exist: low-Reynolds number modelling and wall functions. These options differ in the way in which the boundary layer at the wall surface is taken into account. The boundary layer consists of an inner layer, including the thin viscous sublayer, the buffer layer and the logarithmic layer, and a fully turbulent outer layer [18,19]. Low-Re number modelling refers to resolving the whole boundary layer by placing cells in each part of it. Because the thickness of the viscous sublayer decreases with increasing flow Re number and the Re numbers for wind flow around buildings are quite large (10^5-10^7), the viscous sublayer at exterior building surfaces can be very thin (10 mm - 100 μm) and a high to very high grid resolution is required close to the walls. Because of the computational cost associated with low-Re number modelling, wall functions are often used instead. They are semi-empirical formulae that bridge the region between the wall and the logarithmic layer, and provide an approximation of the effect of the wall on the mean wind speed, turbulence quantities and temperature in the logarithmic layer. As a result, much coarser grids can be used here. This difference in space discretisation is schematically depicted in Fig. 1.

The grid resolution close to a wall can be characterised by the dimensionless wall distance y^+, which is defined as:

$$y^+ = \frac{u_\tau y_P}{\nu} \tag{8}$$

where y_P is the distance from the centre point P of the wall-adjacent cell to the wall, ν is the kinematic viscosity, and u_τ is the friction velocity (m/s) based on the wall shear stress τ_w (Pa) and air density ρ (kg/m³):

$$u_\tau = \sqrt{\frac{\tau_w}{\rho}} \tag{9}$$

An alternative definition of the dimensionless wall distance exists:

$$y^* = \frac{u^* y_P}{\nu} \tag{10}$$

where u* is a friction velocity based on the turbulent kinetic energy k_P in the wall-adjacent cell centre point P and on the constant C_μ:

$$u^* = C_\mu^{1/4} k_P^{1/2} \tag{11}$$

This alternative definition is based on the fact that the ratio $u_\tau^2/k = C_\mu^{1/2}$, where k is the turbulent kinetic energy, is a constant in the logarithmic layer under equilibrium conditions [20]. Note that C_μ appears as a constant in the standard and RNG k-ε model, but that it is variable in the realizable k-ε model. u_τ and u*, and therefore also y^+ and y*, are equal for equilibrium boundary layers. The alternatively defined parameters y* and u* allow to specify grid resolution requirements even at locations in the flow field where τ_w is zero, which occurs at stagnation and reattachment points. In that case, y^+ is zero irrespective of the local grid resolution y_P, and cannot be used to specify the grid requirements. The alternative parameter y*, however, will not be zero because it is based on k_P. Most commercial CFD codes, such as

the one used in the present study, namely Fluent 6.3 [21], express the wall functions in terms of y* instead of y^+, which also results in a qualitative improvement of wall heat transfer [20].

Appropriate grids for low-Re number modelling have a y* value below 4 or 5 to ensure that the centre point P of the wall-adjacent cell is situated in the viscous sublayer. Preferably, y* = 1 to have at least a few cells inside the viscous sublayer [20]. Wall function grids should have a y* above 20-30 and below 300-500 to ensure that P is situated in the logarithmic layer [20,22]. The wall functions are based on the expression of the universal law-of-the-wall in the logarithmic layer. The commercial CFD code Fluent 6.3 that is used in this study provides two types of wall functions: the standard wall functions by Launder and Spalding [23] and the non-equilibrium wall functions by Kim and Choudhury [24]. Strictly, wall functions can only be applied for the conditions for which they have been derived, although they are often also used in other situations. Standard wall functions are valid for attached two-dimensional flow with small pressure gradients, local turbulence equilibrium and a constant near-wall stress layer. Strictly, they are not valid for complex 3D flows with impingement, separation and reattachment, such as flows around buildings. Non-equilibrium wall functions relax the local equilibrium assumption and can partly account for non-equilibrium effects [24]. They can provide better predictions for such complex 3D flows. It is however important to stress that using wall functions can easily compromise the accuracy of surface heat and mass transfer calculations in complex 3D flows. The reason is that they do not resolve the viscous sublayer and the buffer layer, in which the largest resistance to surface heat and mass transfer is embedded. Note that Murakami [25], in his 1993 paper on the comparison of turbulence models for building engineering, already correctly indicated that wall functions cannot be expected to perform well for convective heat transfer calculations. Nevertheless, probably because of the very high grid resolution required for low-Re modelling, wall functions have been used in the past to determine CHTC. In the present paper, the performance of standard and non-equilibrium wall functions for forced convective heat transfer at building surfaces will be evaluated by comparison with low-Re number modelling results.

3. CFD validation

CFD simulations based on the RANS equations in combination with a turbulence model require validation, which can be performed by comparison of the CFD results with either full-scale measurements or wind tunnel data. Because full-scale measurements are generally influenced by a much larger number of parameters, wind tunnel measurements are preferred for basic validation studies. Due to lack of available high-resolution wind tunnel data of CHTC at realistic Reynolds numbers for building applications ($Re \sim 10^5$-10^7), a two-part validation study is performed: (1) comparison of simulations and measurements of the velocity field close to the windward surface of a cubic (0.2 m) building model; (2) comparison of simulations and measurements of the CHTC at the windward surface of a cubic (0.05 m) model in a turbulent channel flow at an obstacle Re number of 4.6×10^3.

3.1. Validation of upstream near-field velocity pattern

3.1.1. Wind tunnel measurements

Wind tunnel measurements of mean wind speed and turbulence upstream of a cubic (0.2 m) building model were reported by Minson et al. [26]. The tests were conducted in the wind tunnel of the University of Oxford, at a scale of 1:75, using 2D Laser Doppler Anemometry (LDA). The wind direction was perpendicular to the windward facade. The blockage ratio was 0.5 %. The building Reynolds number can not be determined from the dimensionless measurement results. The undisturbed vertical profiles of mean wind speed and turbulence quantities were measured in the empty wind tunnel (with roughness elements present but without building) at the location where the building would be positioned. These profiles are called “incident” profiles. The measured incident mean wind speed profile is given in Fig. 2 by the black dots. Two important remarks are made here: (1) the mean wind speed measurements by Minson et al. [26] do not seem to fit a single log law, but show the development of an internal boundary layer (IBL) at the lower part. This is most likely due to the absence of roughness elements on the turntable, over which the IBL develops. The development of IBLs in such cases and its importance for CFD modelling have been discussed in [27]. Two different log laws can be fitted to the data, as indicated in Fig. 2 and Table 1. (2) Minson et al. [26] report a full-scale z_0 of 0.6 m, corresponding to a reduced-scale value of 0.008 m. This is more than five times larger than the z_0 corresponding to “log law 2” in Fig. 2. In the CFD simulations, we use the correct measured inlet profiles, i.e. the experimental values in Fig. 2, which correspond to the measurement data taken with the cubic model present. Measurements with the building model present

were made in the building centre plane, at distances of 1H, 0.5H, 0.2H, 0.15H, 0.1H, 0.075H, 0.05H and 0.025H from the windward facade. In addition, measurements were also made at lateral distances of 0.25H and 0.375H from the centre plane, and at 0.2H, 0.1H and 0.05H from the windward facade. Note that the data by Minson et al. [26] were chosen because of the close proximity of the measurement locations to the facade. More details on the measurements can be found in [26].

3.1.2. CFD simulation and validation

3D steady RANS simulations are performed at model scale and in a computational domain with a blockage ratio of 0.4 %. A hybrid hexahedral-prismatic grid is used with grid resolution determined by grid-sensitivity analysis on three different grids with a refinement factor √2. The resulting grid has 824,232 cells. A high grid resolution near the facade (y_P = 100 μm) is required to have y* < 4 at all positions, for a reference wind speed U_H at cube height of 1 m/s, yielding a building Reynolds number Re_b = 13,700. The incident mean wind speed profile is used as inlet profile, which requires horizontal homogeneity in the simulations, i.e. that the inlet and incident profile are the same. The vertical inlet profiles of turbulent kinetic energy and turbulence dissipation rate are those by Richards and Hoxey [28], based on z_0 and u_{ABL}* from the internal boundary layer (log law 1; Table 1). The sides and the top of the computational domain are modelled as slip walls (zero normal velocity and zero normal gradients of all variables). At the outlet, zero static pressure is specified. For the walls, low-Re number modelling is used. In Fluent 6.3.26, low-Re number modelling implies that the walls are smooth (roughness height k_S = 0), which is also the case for the bottom of the domain. A smooth bottom surface can lead to a non-horizontally homogeneous atmospheric boundary layer in the simulations [29], and, thus, streamwise gradients can occur in the vertical profiles of mean wind speed and turbulence quantities. The occurrence of these gradients was tested by a simulation in an empty 2D domain and was found very limited in this case (< 5 %), due to the very low value of z_0 (log law 1). Therefore this occurrence does not compromise the validation study. The commercial CFD code Fluent 6.3.26 is used to solve the 3D RANS equations using the control volume method. Closure is obtained using the realizable k-ε model by Shih et al. [30], as convergence could not be obtained with the Reynolds Stress model (RSM) by Launder et al. [31] when the grid resolution was below 0.01H near the building facade. Note that for low-Re number modelling, a two-layer zonal approach is used, with the realizable k-ε model in the outer zone and the one-equation Wolfhstein model [32] in the near-wall region. Pressure-velocity coupling is taken care of by the SIMPLE algorithm. Pressure interpolation is standard. Second order discretization schemes are used for both the convection terms and the viscous terms of the governing equations.

Fig. 3a indicates the vertical lines in the building centre plane along which the calculated and measured mean wind speed results are presented in Figs. 3b-d. A fairly good agreement between simulations and measurements is observed. The simulations reproduce the decrease of U/U_H as the wind approaches the windward facade. Also the increase of the absolute value of W/U_H towards the building facade is predicted. The shapes of the U/U_H and W/U_H profiles are well reproduced, but the streamwise wind speed is somewhat underestimated between x/H = -0.5 and -0.025, and the vertical wind speed is underestimated near ground-level. Additional results, outside of the centre plane, are given in Fig. 4. Both the measurements and the simulations show the increase of U/U_H towards the edges of the building model and the negligible change of W/U_H with increasing distance from the centre plane. The underestimation of U/U_H and that of W/U_H near ground-level, which were observed in the centre plane in Fig. 3b-d, are also present outside the centre plane (Figs. 4b-g). In spite of these discrepancies, a good overall agreement is obtained. The same set of computational parameters (turbulence model, low-Re model, discretisation schemes, pressure-velocity coupling, etc.) will therefore be used for the simulations in the next section.

3.2. Validation of convective heat transfer

Because of space limitations, this validation study is only briefly reported here. A detailed report can be found in Defraeye et al. [33].

Meinders [34] and Meinders et al. [35] determined the CHTC at the surfaces of a 0.015 m cube in developing turbulent channel flow using – among others – infrared thermography. The channel has a height of 0.05 m and a depth of 0.6 m. For the validation study, the data for an obstacle Reynolds number of 4.6×10^3 is considered. More information on the experimental setup and the procedure to obtain the temperature and CHTC data from the measurements can be found in Meinders [34]. 3D steady RANS CFD simulations were made at model scale in a computational domain representing the wind tunnel. The realizable k-ε model in combination with the Wolfhstein low-Re number model was used on a high-

resolution grid of about $8x10^5$ cells. All other settings and parameters are the same as those in the previous validation study. The detailed results are reported in [33]. Fig. 5 shows a comparison between the calculated and measured CHTC, along a vertical and a horizontal line on the windward surface (wind direction is perpendicular to the surface). Note that the values at the outer edges are not included in this comparison, because of inaccuracies in the experimental CHTC at these locations [33]. These inaccuracies can be attributed to the procedure that was used to convert the infrared surface temperature measurements to CHTC values. For this, Finite Volume Method (FVM) calculations were employed, that used the temperature boundary conditions on the interior and exterior surfaces of the hollow cube as input parameters. However, the resolution of the temperature measurements was limited to about 30x30 points [34], uniformly distributed on each surface. This resolution results in not more than 3 points over an edge region and is rather low in contrast to the numerical simulations. The discrepancy at the edges could be explained by the low resolution in these zones. This is confirmed by the fact that the CFD simulations of the surface temperatures in the present study show a good agreement with the measured surfaces temperatures, also at the outer edges, while this is not the case for the CTHC. More detailed information can be found in [33].

In spite of these inaccuracies, the agreement between the simulated and the measured CHTC at the other positions, however, is very close, and generally within 10%. This demonstrates that the combination of realizable k-ε model, low-Re Wolfhstein model and all other computational parameters in the two validation studies can yield reliable results for the windward facade. The same set of parameters will therefore be used in the next section.

4. CFD application

The cubic (10 m) building is placed in a computational domain with dimensions $L_D x B_D x H_D$ = 210x210x100 m³. The building is placed at a distance of 5H (= 50 m) from the inlet plane(s) [22]. Two different grids are constructed: grid A is the high-resolution (low-Re number) grid with y_P = 160 μm and 1,880,576 cells, and grid B is the coarser wall-function grid with y_P = 0.01 m and 818,816 cells. Grid A is shown in Fig. 6. The vertical boundary planes of the domain have different types of boundary conditions depending on the wind direction (Fig. 6). For $\theta = 0°$, plane 1 is the inlet plane, plane 3 the outlet plane and planes 2 and 4 are the side planes. For $\theta \neq 0°$, planes 1 and 2 are the inlet planes, and planes 3 and 4 are the outlet planes. At the inlet plane(s), the vertical profiles of mean wind speed, turbulent kinetic energy k and turbulence dissipation rate ε are imposed. The two side planes (for $\theta = 0°$) and the top of the computational domain are modelled as slip walls (zero normal velocity and zero normal gradients of all variables). At the outlet(s), zero static pressure is specified. The inlet conditions are those of a neutral atmospheric boundary layer over a grass-covered terrain with an aerodynamic roughness length z_0 = 0.03 m. Four different reference wind speed values at building height are used: U_{10} = 1, 2, 3 and 4 m/s, yielding building Reynolds numbers $Re_b = 0.7x10^6$, $1.4x10^6$, $2.1x10^6$ and $2.7x10^6$. Nine wind directions are considered: $\theta = 0°$, 11.25°, 22.5°, 33.75°, 45°, 56.25°, 67.5°, 78.75° and 90°, where 0° is perpendicular to the facade (Fig. 6). In all these simulations, the longitudinal turbulence intensity I_u that is imposed at the inlet ranges from 20% at ground level to 5 % at gradient height. The inlet turbulent kinetic energy (k) is calculated based on I_u and the hypothesis of isotropic turbulence, which is implicit to the realizable k-ε model: $k = ½(\sigma_u^2 + \sigma_v^2 + \sigma_w^2) = 3/2(\sigma_u^2) = 3/2(I_u U)^2$. The turbulence dissipation rate is taken as $\varepsilon = u^{*3}/\kappa(z+z_0)$ where u^* is the friction velocity, κ the von Karman constant (~ 0.42) and z the height co-ordinate. The bottom of the domain is modelled as a no-slip wall with zero roughness height k_S = 0. Although k_S should actually be determined from z_0 using the appropriate relation for consistency between inlet profiles and wall functions [29], here it has to be set to zero in order not to disturb the comparison of the CHTC obtained from low-Re number modelling versus wall-function modelling. The reason is that roughness can only be set when using wall functions in Fluent 6.3, while low-Re modelling assumes zero roughness. Although zero roughness at the bottom of the domain will lead to streamwise gradients of the vertical mean wind speed and turbulence profiles (horizontal inhomogeneity) [29], these gradients will occur in both cases (wall functions and low-Re modelling) and will therefore not influence the comparison. However, given the horizontal homogeneity, it is important to mention the incident profiles, i.e. the profiles to which the building model is actually subjected. These are the profiles that would occur at the position of the building, if the building were absent [27,29]. The inlet profiles and incident profiles for U_{10} = 3 m/s are shown in Fig. 7a and b. Although horizontal inhomogeneity is limited for the mean wind speed profile, it is very pronounced for k and I_u: Fig. 7b shows that the maximum value of I_u drops from 18 % at the inlet to almost 10 % at the virtual position of the building. Given the

important influence of turbulence on the CHTC, as will be shown in sections 5.3 and 6.2, this issue should be borne in mind when interpreting and using the results of this study.

The thermal boundary conditions are a fixed building surface temperature of 303 K, an inlet air temperature of 283 K and the bottom of the computational domain is an adiabatic wall. The reference temperature to determine the CHTC is the inlet temperature (283 K). Although the turbulent Prandtl number might vary somewhat with the local flow conditions, it is kept at its default value $Pr_t = 0.85$. Only forced convection is taken into account. This situation can be considered physically valid when the ratio Gr/Re^2 is well below 0.2 [36]. For grid A, the realizable k-ε model is used together with the low-Re number Wolfhstein model. For grid B, the realizable k-ε model is used in combination with either the standard or non-equilibrium wall functions mentioned in section 2. Pressure-velocity coupling is taken care of by the SIMPLE algorithm. Pressure interpolation is standard. Second order discretization schemes are used for both the convection terms and the viscous terms of the governing equations. The iterations for all simulations were continued until no further decrease of the scaled residuals [21] could be obtained. Note that the default threshold of 0.001 that is recommended by the Fluent 6 manual [21] should not be trusted without carefully checking whether the solution still changes significantly if additional iterations are performed. It has been found during simulations for this paper that, especially for high-resolution grids and with constant value initialisation, this default threshold is by far too lenient, and the CHTC values that are obtained at this stage are overestimated by more than 100 % compared to the fully converged values. The fully converged simulations show that the low-Re number grid A has $y^* < 4$ at all facade positions and the wall-function grid B has $30 < y^* < 300$ at the windward facade. The simulation results are presented in the next section.

5. Results

Prior to the presentation and the discussion of the results, it is noted that steady RANS modelling, as applied in this paper, is not capable of modelling the inherently transient nature of separation and recirculation that occur downstream of the windward facade, and of von Karman vortex shedding in the wake. Calculation results in the downstream regions are therefore generally deficient [25,37]. However, steady RANS with the realizable k-ε model has been shown adequate for the calculation of the mean wind speed upstream of the building facade and for the calculation of the CHTC for the windward face of a reduced-scale cube (see section 3). For these reasons, this paper mainly focuses on the results at the windward facade, and results for the other facades and the roof should be treated with caution.

5.1. CHTC distribution across the facade

The CHTC distribution across the windward facade, calculated with low-Re number modelling, is displayed in Fig. 8 for $U_{10} = 3$ m/s and for $\theta = 0$, 22.5, 45 and 67.5°. In all cases, the CHTC shows an overall increase from bottom to top, and from the middle of the facade to the sides. The highest values are found at the top edges. This is attributed to the local flow acceleration at these locations that reduce the thickness of the boundary layer. The CHTC gradients also increase towards the top of the facade. The CHTC distribution pattern does not show major changes with a change in wind direction. More information is provided in Fig. 9 that presents the values of the CHTC along the perimeter of a vertical and a horizontal cross-section by a plane cutting midway through the building. It confirms the relative insensitivity of the CTHC distribution at the windward facade to wind direction changes. At the other facades, the influence of wind direction is more pronounced. The results at these facades however should be treated with caution, as mentioned before, because they have been obtained with steady RANS. Nevertheless, the CFD simulations predict a fairly uniform CHTC distribution in the wake (line 2-3 in Fig. 9a), similar to what has been found in experiments in the past [35,38,39].

5.2. Low-Re number modelling versus wall functions

So far, all CFD simulation results presented in this paper have been obtained by low-Re number modelling. Previous CFD simulations of exterior CHTC for buildings were made using wall functions [16]. Wall functions allow avoiding high-resolution computational grids and are computationally less expensive and faster. For example, for the simulation in this paper, the smallest wall-adjacent cells in the low-Re number grid ($y_P = 160$ μm) are about 60 times finer than those in the wall-function grid ($y_P = 0.01$ m). For building engineering applications, wall-function grids are easier to construct and generally provide better convergence behaviour, because the difference between the minimum and maximum cell

sizes in the computational domain is much smaller. However, as mentioned before, wall functions are based on certain assumptions. Generally, they should not be used for those simulations in which the accurate modelling of near-wall processes is crucial, which is the case for convective heat and mass transfer at surfaces. A comparison between results for the CHTC, obtained using low-Re number modelling on grid A and wall-function modelling on grid B, is shown in Fig. 10 (for U_{10} = 3 m/s and θ = 0°). At the windward facade, using standard wall functions yields overestimations up to 60% compared to low-Re modelling, while non-equilibrium wall functions give overestimations up to 30%. As expected, the non-equilibrium wall functions, which can partly take into account non-equilibrium boundary layer behaviour, perform better than the standard wall functions, but are still insufficiently accurate for convective heat transfer calculations.

5.3. Correlations[1] at fixed facade positions

At fixed positions at the facade, correlations between the CHTC and various relevant parameters can be investigated. Previous researchers [8,13,14,15] presented experimentally obtained correlations between h_c and local wind speed $V_{3D,loc}$, between h_c and the reference wind speed U_{10}, and between $V_{3D,loc}$ and U_{10}. A similar analysis can be made based on the CFD results. In addition, the turbulent kinetic energy k is included in the analysis. The reason is the importance of turbulence for convective heat transfer.

5.3.1. Correlation between U_{10} and $V_{3D,loc}$

For $V_{3D,loc}$, two distances from the facade are considered, inspired by those mentioned in the literature overview in section 1: d = 0.3 m and d = 1 m. This allows comparison with the results by other researchers. Results are presented for four points on the facade (Fig. 11): p1 (x' = 0.5 m; y' = 9.5 m), p2 (5;9.5), p3 (0.5;5) and p4 (5.5). For d = 0.3 m, Fig. 11 indicates that at every facade position and for every wind direction, there is a different linear correlation between $V_{3D,loc}$ and U_{10}. This is also the case for other distances d and other facade positions. For isothermal flows around bluff bodies with sharp edges, where the positions of flow separation are located at those edges and are therefore independent of the Reynolds number, the relationship between the wind speed at any location in the flow field and a reference wind speed is indeed generally taken to be linear. This corresponds to wind engineering practice, in which wind-velocity patterns around buildings are generally only measured (in the wind tunnel) or calculated (with CFD) for a single reference wind speed. This is also reflected in the concept of the pressure coefficient ($C_p = (P-P_{ref})/0.5\rho U_{ref}^2$) that is typically determined for a given value of the reference wind speed U_{ref}, and subsequently used for the entire range of possible reference values. Fig. 11 also shows that the correlation between $V_{3D,loc}$ and U_{10} is strongly dependent on the facade location and the wind direction. Similar observations are found for d = 1 m. This corresponds to the statements by Sharples [13].

5.3.2. Correlation between h_c and $V_{3D,loc}$

Heat transfer theory predicts power-law correlations between h_c and $V_{3D,loc}$, and such correlations are also found in this study. Fig. 12a displays h_c as a function of $V_{3D,loc}$ at d = 0.3 m from the facade, for four different facade positions. Fig. 12b shows the correlation between the same parameters, at the top corner of the facade, for different wind directions. Fig. 12c and d show the same for d = 1 m. These correlations are provided in Tables 2 and 3 together with their coefficients of determination. The correlations are very different depending on the facade position (see e.g. point p4 in Figs. 12a and c) and on wind direction. This corroborates the findings by Sharples [13], and his comments on the conclusions by Ito et al. [8], who found the opposite. The fact that the correlations also vary significantly with wind direction explains - at least partly - the scatter and the relatively low coefficients of determination (R^2) found by previous researchers that grouped results into the broad categories "windward" ($-90° < \theta < 90°$) and "leeward". Previous attempts also tried to correlate h_c and U_{10}. Combining the observations from sections 5.3.1 and 5.3.2 however indicates that no good correlation can be expected between h_c and U_{10}, unless the wind direction is fixed within a tight interval.

[1] Strictly, the word *correlation* refers to the strength and direction of a *linear* relationship between two variables. In experimental and theoretical heat transfer theory, it is often used to indicate any type of relationship, not necessarily linear. This more general interpretation is also used in this paper.

5.3.3. Correlation between h_c and $k^{0.5}$

Because of the importance of turbulence for convective heat transfer, correlations between h_c and an alternative velocity scale, namely the square root of the turbulent kinetic energy, $k^{0.5}$ (m/s), are explored. Fig. 13a-d and Tables 4-5 show that also here, power-law correlations are obtained with high coefficients of determination. In addition, Fig. 13a shows that, for $\theta = 0°$, nearly the same correlation is found for all four different facade positions. This is also true for $\theta = 22.5$, 45 and 67.5° (not shown in figure). Fig. 13c shows that the correlations deviate more when k is taken at a larger distance from the facade (d = 1 m), but this deviation is still less than in Fig. 12c. Overall, the h_c-$k^{0.5}$ correlations seem to be less variable across the facade than the h_c-$V_{3D,loc}$ correlations. As Fig. 12b and d, also Fig. 13b and d show the strong influence of wind direction.

5.3.4. Correlation between surface-averaged h_c and U_{10}

Fig. 14a and Table 6 show the power-law correlation between the CHTC, averaged over the entire windward surface, and U_{10}. Fig. 14b displays the variation of the CHTC with wind direction. It shows that at least the surface-averaged CHTC is relatively insensitive to wind direction changes within the interval [0°; 67.5°]. This variation can be described by the following correlation with $R^2 = 0.9989$:

$$h_c = 10.74 \cos^3\theta - 22.06 \cos^2\theta + 16.48 \cos\theta + 7.14 \quad (12)$$

5.4. Correlations across the facade

Fig. 8 has shown that the CHTC reaches its highest values at positions where also the local wind speed is high, i.e. near the top edge and the vertical side edges of the windward building facade(s). Although this might indicate that the correlations between the CHTC and $V_{3D,loc}$ are quite similar across the facade, Fig. 12a and c have shown that that this is not the case for at least the middle area of the facade. Fig. 13a and c suggested that the spatial correlation between the CHTC and $k^{0.5}$ is higher than between the CHTC and $V_{3D,loc}$. Fig. 15 shows these correlations across the windward facade, for $U_{10} = 3$ m/s, for d = 0.3 m and 1 m, and for $\theta = 0°$ and 45°. While the correlations between h_c and $V_{3D,loc}$ are low, those between h_c and $k^{0.5}$ are relatively high, especially for $\theta = 0°$.

5.5. CHTC and wind-driven rain

Fig. 16 compares the spatial distribution of the CHTC at the windward facade with previous validated simulation results of the wind-driven rain (WDR) catch ratio η [40] at the same windward facade [41,42]. The catch ratio is defined as the WDR intensity on the building facade, divided by the reference horizontal rainfall intensity R_h (i.e. the intensity falling on the ground). Both the CHTC and WDR are shown for $U_{10} = 3$ m/s and $\theta = 0°$. Both spatial distributions show a strong similarity, with both CTHC and η increasing from bottom to top, and from the middle to the sides, with maximum values at the top edge and top corners. Since the CHTC is related to the CMTC, also the CMTC will probably reach its highest values at the top of the facade. This means that the facade parts that receive most WDR might also experience a higher drying rate.

6. Discussion

6.1. Limitations of this study

High-resolution 3D steady RANS CFD simulations of wind flow and forced convective heat transfer for a 10 m cubic building have been presented. This study has some important limitations:

- Steady RANS modelling can not capture the inherently transient behaviour of flow separation, recirculation and von Karman vortex shedding occurring downstream of the windward facade. Therefore, the focus of this study was on the windward facade. CFD validation showed good results for mean wind speed and CHTC at the windward surface of reduced-scale cubic obstacles. The results for the other surfaces should not be considered accurate and should be treated with caution. Future studies should employ improved turbulence modelling, using Detached Eddy Simulation (DES) or Large Eddy Simulation (LES), to also provide accurate information for the other building surfaces.

- The occurrence of streamwise gradients in the vertical profiles of turbulent kinetic energy and turbulence intensity implies that the derived correlations and results in this paper are representative for the incident flow conditions, with $I_{u,max}$ = 10%, i.e. a very smooth upstream terrain. They are not representative for the inlet flow conditions.
- The building facade has been assumed to be perfectly smooth. Earlier experimental studies have shown the importance of small-scale surface roughness on convective heat transfer [43,44]. For example, Rowley et al. [43] found that the CHTC for stucco was almost twice that for glass. Other studies showed the important influence of larger-scale surface roughness, such as the presence of mullions in glazed areas or architectural details on the facade, on the CHTC [45,46].
- Only forced convection has been considered. This is considered appropriate when the ratio Gr/Re^2 is well below 0.2. Further research will include mixed convection.
- The realizable k-ε model and the Boussinesq hypothesis assume isotropic turbulence. Further research is necessary to analyse correlations between the CHTC and the turbulent kinetic energy when the anisotropy of the Reynolds stress tensor is taken into account.
- Grid resolution requirements were based on the thickness of the momentum boundary layer (BL). Since for air flow the molecular Prandtl number is about 0.74, the thermal BL will generally be larger than the momentum BL, and the grid resolution is also considered appropriate for the thermal BL. However, further studies are needed to corroborate this for the case of complex 3D flows with impingement, separation and recirculation.
- Only one (simple) building configuration was studied here. Future CFD studies should focus on different building configurations in different environment topographies.

6.2. Comparison with previous CFD study

For the surface-averaged CHTC on the windward facade, the present study provides the correlations in Table 6, with $h_c = 4.6U_{10}^{0.89}$ for $\theta = 0°$. A previous study [16] also presented CFD results of the surface-averaged CHTC as a function of U_{10}, also for a low-rise building. Their result is $h_c = 5.15U_{10}^{0.81}$ for $\theta = 0°$. The results from both studies are quite similar, which is surprising because the present study used low-Re number modelling, while the other study used wall functions. As shown in Fig. 10, standard or non-equilibrium wall functions can significantly overestimate the actual CHTC, by up to 60% and 30%, respectively. The fact that, in spite of this, similar results are obtained, could be explained as follows. The study by Emmel et al. [16] did not report the inlet turbulence intensity for the simulations. From a similar study by these authors [47] that seems to have used the same CFD calculations, it can be seen (Fig. 11 in [47]) that the approach flow turbulence intensity is only 1 %. This, unfortunately, is an unrealistically low value for flow in the atmospheric boundary layer. To investigate whether using this low value could have compensated the error caused by the wall functions, in this study simulations with different incident turbulence intensities for the 10 m cubic building are performed. The results are given in Table 7. It shows that using an incident turbulence intensity of 1.5 % instead of 10.5 % yields an underestimation of the CHTC by about 66 %. Therefore, it is expected that both errors in the wall-function simulations in [16] have cancelled each other out, and that this is the reason why those wall-function simulations provide almost the same averaged CHTC correlations as the low-Re number simulations from the present study.

6.3. Correlations with local wind speed versus local turbulent kinetic energy

The influence of turbulence on the CHTC, shown by Table 7, is also confirmed by the correlations between h_c and $k^{0.5}$ that have been presented. These correlations appear more universal than the traditional correlations between h_c and $V_{3D,loc}$. The fact that k appears to be a more important factor than $V_{3D,loc}$ in determining the CHTC is corroborated by the experimental observations that the CHTC increases with increasing small-scale surface roughness [43,44]. As this roughness increases, the local wind speed near the surface in the boundary layer $V_{3D,loc}$ will decrease [18], while k will increase. The increase in k appears dominant compared to the decrease in $V_{3D,loc}$, since the overall result is an increase of h_c. A tentative conclusion is that $k^{0.5}$ is more suitable as a velocity scale than $V_{3D,loc}$ in CHTC correlations. This however will need to be confirmed by CFD simulations that take into account turbulence anisotropy. Note that, while using k might seem less practical than $V_{3D,loc}$, both parameters can be measured quite easily and accurately with a high-temporal-resolution 3D anemometer (e.g., ultrasonic anemometer).

6.4. Feasibility of using CFD for urban CHTC predictions

The necessity of low-Re number modelling for convective heat and mass transfer calculations and the high Re numbers associated with wind flow around buildings require using high-resolution grids with a large number of cells, even for isolated buildings. When multiple buildings or even part of a city is involved, as in urban CFD simulations, the grids will become too large and too computationally expensive. For those situations, specially-adapted wall functions will need to be devised.

7. Conclusions

High-resolution 3D steady RANS CFD simulations of forced convective heat transfer at the facades of a low-rise cubic (10 m) building have been performed to determine convective heat transfer coefficients (CHTC). The focus has been on the windward facade. The following conclusions are made:

- CFD validation based on wind tunnel measurements has shown that the high-Re number realizable k-ε model in combination with the low-Re number Wolfhstein model can provide accurate results for mean wind velocity and convective heat transfer at the windward surface of reduced-scale cubic models.
- Low-Re number CFD simulations for the 10 m cubic building required a high-resolution grid with cell centres at a minimum distance of 160 μm (for U_{10} = 3 m/s) from the building surface to resolve the entire boundary layer, including the viscous sublayer and the buffer layer, which dominate the convective surface resistance. These simulations showed that:
  1. The wind flow around the building results in highly varying CHTC values across the windward facade.
  2. Standard and non-equilibrium wall functions are not suitable for CHTC calculation; for the windward facade they provide overestimations up to 60 and 30 %, respectively. Either low-Reynolds number modelling or specially-adapted wall functions should be used instead.
  3. At every facade position, the CHTC is a power-law function of the mean wind speed.
  4. The CHTC distribution at the windward facade, and therefore also the surface-averaged CHTC for this facade, are relatively insensitive to wind direction variations within the interval [0;67.5°].
  5. The spatial correlation between the local CHTC and the local turbulent kinetic energy is better than that between the local CHTC and the local mean wind speed at a certain distance from the facade.
  6. The CHTC distribution across the windward facade is quite similar to the distribution of wind-driven rain (WDR), with both parameters reaching high levels near the top edge of the facade. This suggests that also the convective moisture transfer coefficient will be higher at this location and that the facade parts that receive most WDR might also experience higher drying rates.
- The results for facades other than the windward facade, as presented in this paper, should be treated with caution. The reason is that steady RANS is incapable of capturing the inherently transient behaviour of separation and recirculation downstream of the windward facade and of von Karman vortex shedding in the wake. Therefore, (more) accurate results at these surfaces should be pursued using transient simulations with DES or LES.

Acknowledgements

The authors are grateful for the kind assistance by Ir. Twan van Hooff and Ir. Mohammad Mirsadeghi, PhD students at the Unit Building Physics and Systems (BPS) of Eindhoven University of Technology, and for the important computing infrastructure support by Ing. Jan Diepens and Ing. Harrie Smulders, members of the Laboratory of BPS.

Nomenclature

C_μ	variable in realizable k-ε model (-)
C_p	pressure coefficient (-)
d	distance (normal) from the facade (m)
g_v	convective vapour flux density (kg/m²s)
Gr	Grashof number (-)
h_c	convective heat transfer coefficient (W/m²K)

h_m	convective moisture transfer coefficient (s/m)
H	cube height (m)
I_u	longitudinal turbulence intensity (-)
k	turbulent kinetic energy (m^2/s^2)
k_P	turbulent kinetic energy in the wall-adjacent cell centre point P (m^2/s^2)
k_s	physical roughness height (m)
L_D, B_D, H_D	length, width, height of computational domain (m)
$p_{v,ref}$	reference vapour pressure (Pa)
$p_{v,s}$	surface vapour pressure (Pa)
P	centre point of the wall-adjacent cell (-)
P	static pressure (Pa)
P_{ref}	reference pressure (Pa)
Pr_t	turbulent Prandtl number (-)
R_h	horizontal rainfall intensity (mm/h)
R^2	coefficient of determination (-)
Re	Reynolds number (-)
Reb	Building Reynolds number, based on building height H and wind speed U_H
T_{ref}	reference temperature (K)
T_s	surface temperature (K)
u_τ	friction velocity (m/s)
u*	friction velocity (m/s)
u^*_{ABL}	friction velocity associated with the ABL inlet profiles of U, k and ε (m/s)
U, V, W	streamwise, lateral and vertical component of the mean wind-velocity vector (m/s)
U_{10}	reference wind speed (streamwise) at 10 m height in the upstream undisturbed flow (m/s)
U_H	reference wind speed (streamwise) at building height in the upstream undisturbed flow (m/s)
U_{ref}	reference wind speed (m/s)
$V_{3D,loc}$	magnitude of the local 3D velocity vector at a certain distance from the facade (m/s)
V_R	wind speed measured at some height above the roof (m/s)
V_∞	free-stream velocity in wind tunnel (m/s)
x, y, z	Cartesian co-ordinates (m)
y_P	distance from the centre point P of the wall-adjacent cell to the wall (m)
y^+	dimensionless wall distance (-)
y*	dimensionless wall distance (-)
z_0	aerodynamic roughness length (m)
ε	turbulence dissipation rate (m^2/s^3)
η	wind-driven rain catch ratio (-)
θ	angle between wind direction and normal to the wall (°)
κ	von Karman constant (≈ 0.42)
ν	kinematic viscosity of air (m^2/s)
ρ	density of air (kg/m^3)
σ_u, σ_v, σ_w	standard deviation of turbulent fluctuations in x, y, z direction (m/s)
τ_w	wall shear stress (Pa)
ABL	Atmospheric Boundary Layer
CFD	Computational Fluid Dynamics
CHTC	Convective Heat Transfer Coefficient
CMTC	Convective Moisture Transfer Coefficient
HAM	Heat-Air-Moisture
RANS	Reynolds-Averaged-Navier-Stokes (equations)
WDR	Wind-Driven Rain

References

[1] Steeman HJ, Janssens A, Carmeliet J, De Paepe M. Modelling indoor air and hygrothermal wall interaction in building simulation: Comparison between CFD and a well-mixed zonal model. Building and Environment 2009; 44(3): 572-583.
[2] Chilton TH, Colburn AP. Mass transfer (absorption) coefficients. Industrial and Engineering Chemistry 1934; 26: 1183-1187.
[3] Masmoudi W, Prat M. Heat and mass transfer between a porous medium and a parallel external flow. Application to drying of capillary porous materials. International Journal of Heat and Mass Transfer 1991; 34: 1975-1989.
[4] Derome D. Moisture occurrence in roof assemblies containing moisture storing insulation and its impact on the durability of the building envelope. Ph.D Thesis, Concordia University, Montreal, 1999.
[5] Wadsö L. Surface mass transfer coefficients for wood. Drying Technology 1993; 11: 1227-1249.
[6] Jürges W. Der Wärmeübergang an einer ebenen Wand (heat transfer at a plane wall). Beihefte zum Gesundheits-Ingenieur 1924; 1 (19).
[7] CIBS. Chartered Institute of Building Services Guide Book A, Section A3. London, 1979.
[8] Ito N, Kimura K, Oka J. A field experiment study on the convective heat transfer coefficient on exterior surface of a building. ASHRAE Transactions 1972; 78: 184-191.
[9] ASHRAE. ASHRAE Task Group. Procedure for determining heating and cooling loads for computerising energy calculations. Algorithms for building heat transfer subroutines. New York, 1975.
[10] Wise AFE, Sexton DE, Lillywhite MST. Studies of air flow round buildings, The Architects' Journal 1965; 141: 1185–1189.
[11] Sexton DE. Building Aerodynamics. Current Paper 64/68, Building Research Station, 1968.
[12] Wise AFE. Wind Effects Due to Groups of Buildings, In: Proceedings of the Royal Society Symposium Architectural Aerodynamics, Session 3, Effect of Buildings on the Local wind, London. pp. 26–27 February, 1970.
[13] Sharples S. Full scale measurements of convective energy losses from exterior building surfaces. Building and Environment 1984; 19: 31-39.
[14] Loveday DL, Taki AH. Convective heat transfer coefficients at a plane surface on a full-scale building facade. International Journal of Heat and Mass Transfer 1996; 39(8): 1729-1742.
[15] Liu Y, Harris DJ. Full-scale measurements of convective coefficient on external surface of a low-rise building in sheltered conditions. Building and Environment 2007; 42(7): 2718-2736.
[16] Emmel MG, Abadie MO, Mendes N. New external convective heat transfer coefficient correlations for isolated low-rise buildings. Energy and Buildings 2007; 39(3): 335-342.
[17] Janssen H, Blocken B, Carmeliet J. Conservative modelling of the moisture and heat transfer in building components under atmospheric excitation. International Journal of Heat and Mass Transfer 2007; 50(5-6): 1128-1140.
[18] White FM. Viscous fluid flow. Third Edition. McGraw-Hill, 1974.
[19] Wilcox DC. Turbulence modelling for CFD. Second Edition. DCW Industries, 1998.
[20] Casey M, Wintergerste T. ERCOFTAC Special Interest Group on "Quality and Trust in Industrial CFD": Best Practice Guidelines. ERCOFTAC, 2000.
[21] Fluent Inc. Fluent 6.3 User's Guide. Lebanon, US, 2006.
[22] Franke J, Hellsten A, Schlünzen H, Carissimo B. Best practice guideline for the CFD simulation of flows in the urban environment. COST Action 732: Quality Assurance and Improvement of Microscale Meteorological Models, 2007.
[23] Launder BE, Spalding DB. The numerical computation of turbulent flows. Computer Methods in Applied Mechanics and Engineering 1974; 3: 269-289.
[24] Kim SE, Choudhury D. A near-wall treatment using wall functions sensitized to pressure gradient, ASME FED Vol. 217, Separated and Complex Flows, 1995.
[25] Murakami S. Comparison of various turbulence models applied to a bluff body. Journal of Wind Engineering and Industrial Aerodynamics 1993; 46&47: 21-36.
[26] Minson AJ, Wood CJ, Belcher RE. Experimental velocity measurements for CFD validation. Journal of Wind Engineering and Industrial Aerodynamics 1995; 58: 205-215.
[27] Blocken B, Stathopoulos T, Carmeliet J. Wind environmental conditions in passages between two long narrow perpendicular buildings. Journal of Aerospace Engineering 2008; 21(4): 280-287.
[28] Richards PJ, Hoxey RP. Appropriate boundary conditions for computational wind engineering models using the k-ε turbulence model. Journal of Wind Engineering and Industrial Aerodynamics 1993; 46&47: 145-153.

[29] Blocken B, Stathopoulos T, Carmeliet J. CFD simulation of the atmospheric boundary layer: wall function problems. Atmospheric Environment 2007; 41(2): 238-252.
[30] Shih TH, Liou WW, Shabbir A, Zhu J. A new k-ε eddy-viscosity model for high Reynolds number turbulent flows – model development and validation. Computers and Fluids 1995; 24(3): 227-238.
[31] Launder BE, Reece GJ, Rodi W. Progress in the development of a Reynolds-stress turbulence closure. Journal of Fluid Mechanics 1975; 68(3): 537–566.
[32] Wolfhstein M. The velocity and temperature distribution of one-dimensional flow with turbulence augmentation and pressure gradient. International Journal of Heat and Mass Transfer 1969; 12: 301-318.
[33] Defraeye T, Blocken B, Carmeliet J. 2009. CFD analysis of convective heat transfer at the surfaces of a cube in a deep turbulent boundary layer. Submitted.
[34] Meinders ER. Experimental study of heat transfer in turbulent flows over wall mounted cubes, PhD thesis. Technische Universiteit Delft, Delft, The Netherlands, 1998.
[35] Meinders ER, Hanjalic K., Martinuzzi RJ. Experimental study of the local convection heat transfer from a wall-mounted cube in turbulent channel flow, Transactions of the ASME: Journal of Heat Transfer 1999; 121: 564-573.
[36] Ruck B. Wind-tunnel measurements of flow field characteristics around a heated model building. Journal of Wind Engineering and Industrial Aerodynamics 1993; 50: 139-152.
[37] Tominaga Y, Mochida A, Murakami S, Sawaki S. Comparison of various revised k–ε models and LES applied to flow around a high-rise building model with 1:1:2 shape placed within the surface boundary layer. Journal of Wind Engineering and Industrial Aerodynamics 2008; 96(4): 389-411.
[38] Kelnhofer WJ, Thomas CJ. External convection heat transfer coefficients on a building model. ASME Paper 76-WA/FE-30, ASME Winter Annual Meeting, New York, 1976.
[39] Chyu MK, Natarajan V. Local heat/mass transfer distributions on the surface of a wall-mounted cube. Transactions of the ASME: Journal of Heat Transfer 1991; 113: 851-857.
[40] Blocken B, Carmeliet J. A review of wind-driven rain research in building science. Journal of Wind Engineering and Industrial Aerodynamics 2004; 92(13): 1079-1130.
[41] Blocken B, Carmeliet J. The influence of the wind-blocking effect by a building on its wind-driven rain exposure. Journal of Wind Engineering and Industrial Aerodynamics 2006; 94(2): 101-127.
[42] Blocken B, Carmeliet J. Validation of CFD simulations of wind-driven rain on a low-rise building facade. Building and Environment 2007; 42(7): 2530–254.
[43] Rowley FB, Algren AB, Blackshaw JL. Surface conductances as affected by air velocity, temperature and character of surface. ASHRAE Transactions 1930; 36: 429-446.
[44] Cole RJ, Sturrock NS. The convective heat exchange at the external surface of buildings. Building and Environment 1977; 12: 207–214.
[45] Loveday DL, Taki AH, Versteeg H. Convection coefficients at disrupted building facades – laboratory and simulation studies. International Journal of Ambient Energy 1994: 15(1): 17-26.
[46] Taki AH, Loveday DL. External convection coefficients for framed rectangular elements on building facades. Energy and Buildings 1996; 24: 147-154.
[47] Abadie MO, Mendes N. Numerical assessment of turbulence effect on the evaluation of wind-driven rain specific catch ratio. International Communications in Heat and Mass Transfer 2008; 35(10): 1253-1261.

FIGURES

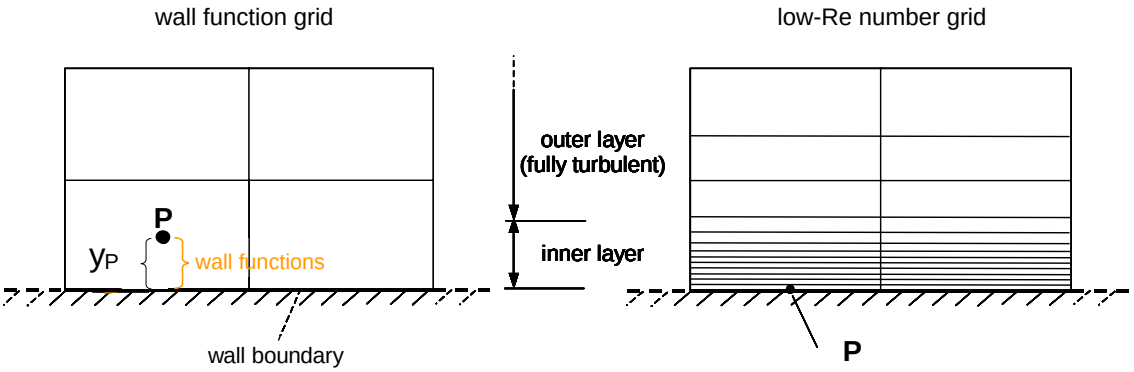

Fig. 1. Schematic representation of part of a grid near a wall boundary. Left: wall function grid. Right: low-Re number grid. P denotes the centre point of a wall-adjacent cell.

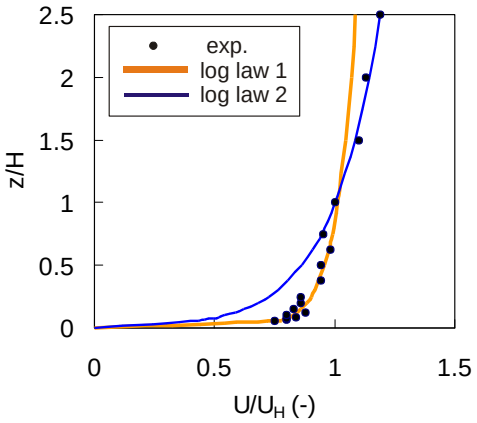

Fig. 2. Vertical profile of incident mean wind speed ratio U/U_H, where U_H is the reference wind speed at cube height. Two log-law profiles can be fitted through the data points, indicating the presence of an internal boundary layer.

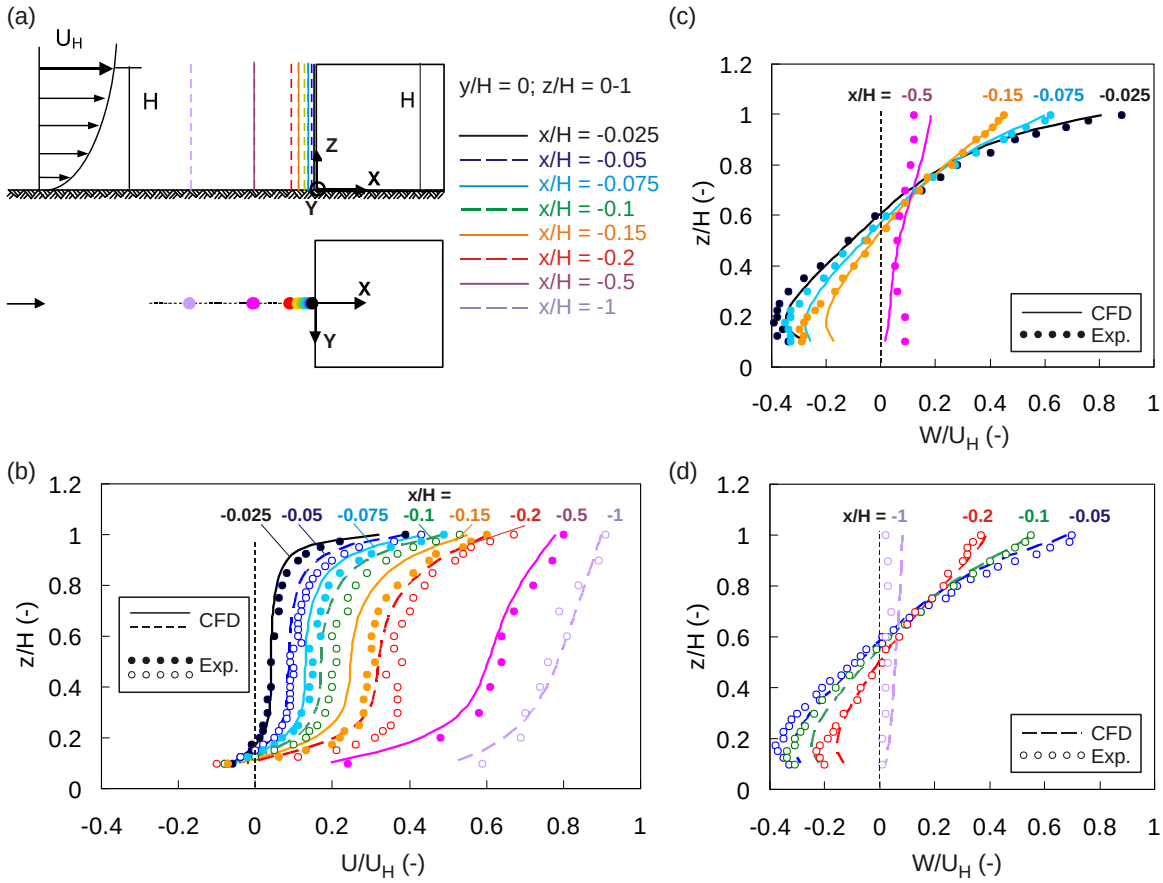

Fig. 3. Comparison between CFD and experimental results for low-rise cubic building: (a) vertical lines along which results are presented; (b) dimensionless streamwise velocity component; (c-d) dimensionless vertical velocity component.

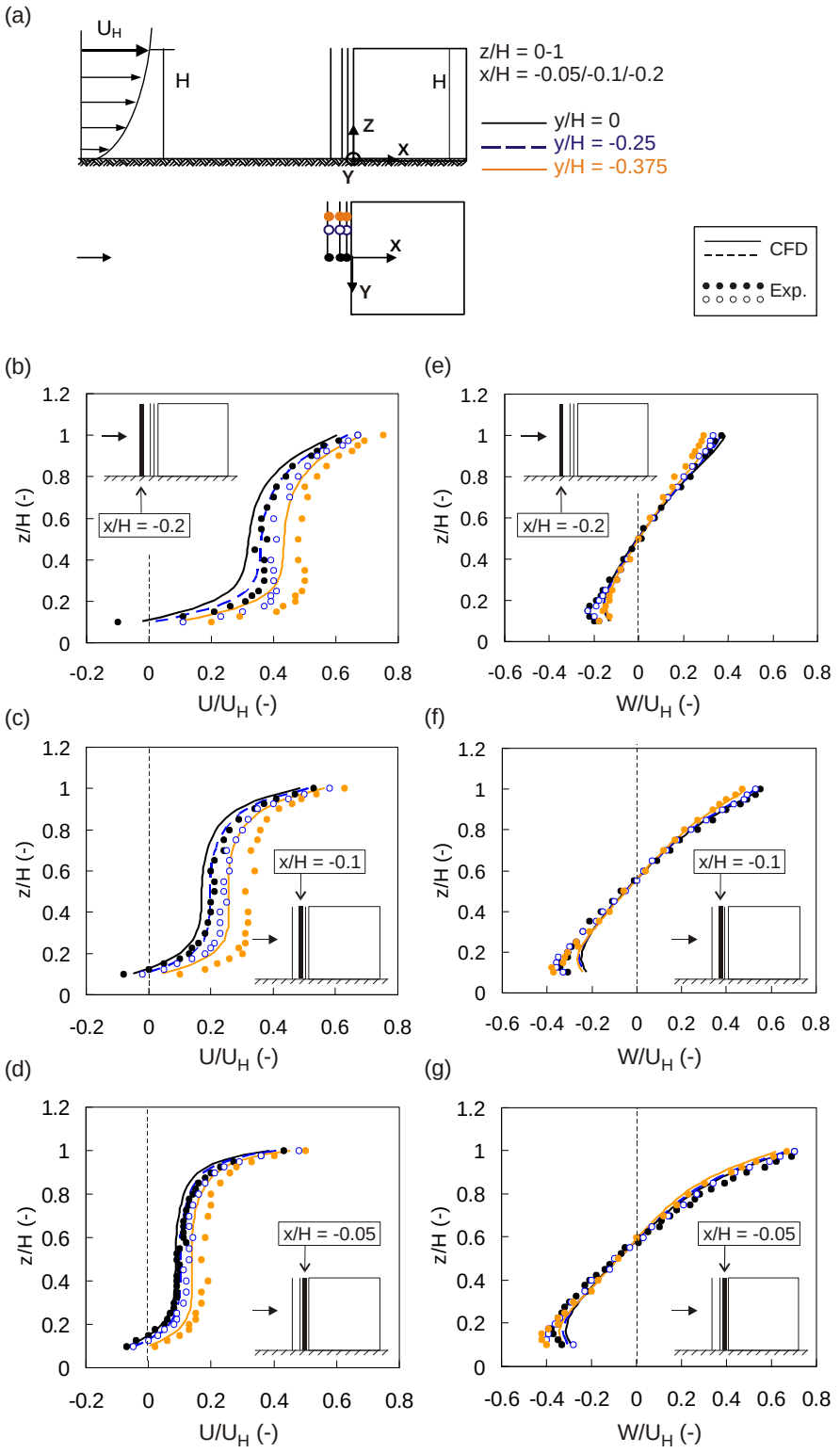

Fig. 4. Comparison between CFD and experimental results for low-rise cubic building: (a) vertical lines along which results are presented; (b-d) dimensionless streamwise velocity component; (e-g) dimensionless vertical velocity component.

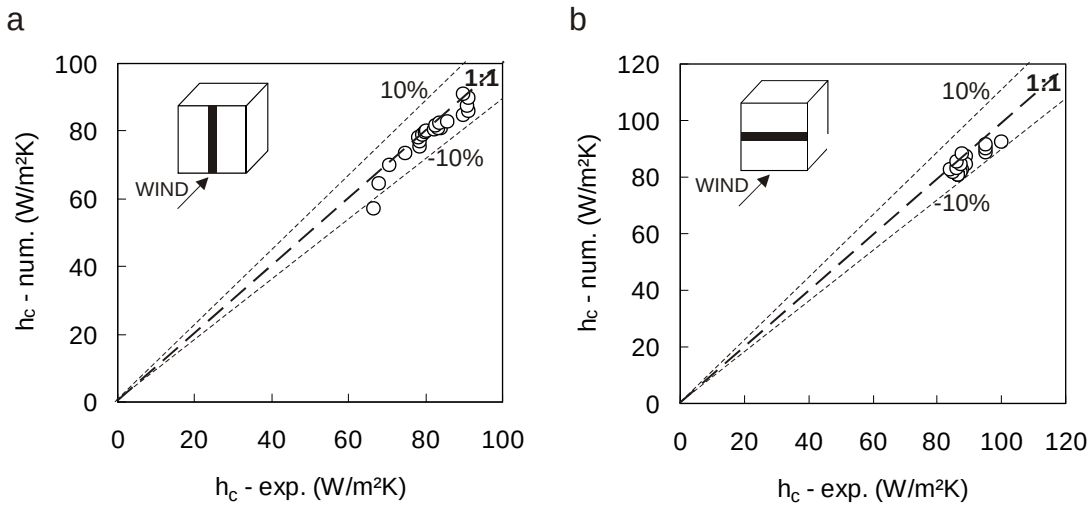

Fig. 5. Comparison of calculated (num.) and measured (exp.) CHTC along (a) a vertical and (b) a horizontal line on the windward surface.

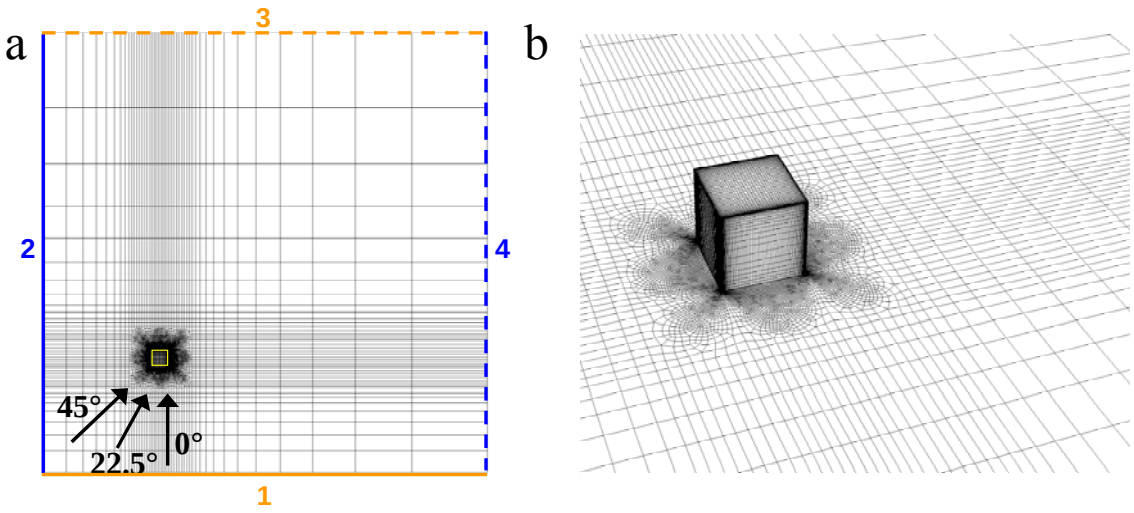

Figure 6. (a) Top view of bottom of computational domain and low-Re grid at the bottom surface. The numbers 1-4 refer to the vertical planes bounding the domain. (b) Perspective view of high-resolution grid at building surfaces and part of the ground surface.

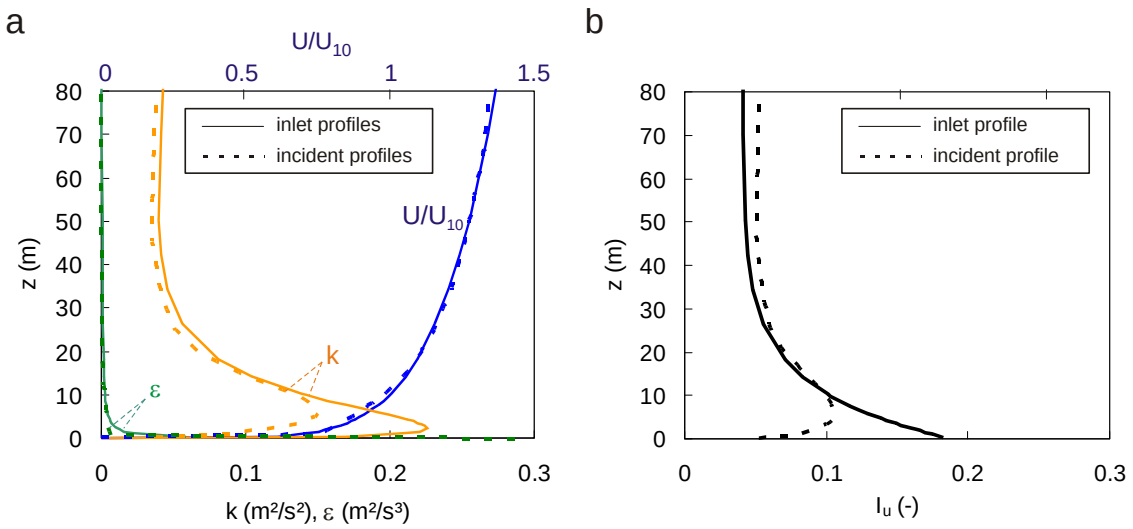

Figure 7. (a) Comparison of inlet and incident vertical profiles of mean wind speed ratio U/U_{10}, turbulent kinetic energy k and turbulence dissipation rate ε in the simulated atmospheric boundary layer, for the case with U_{10} = 3 m/s. (b) Same, for longitudinal turbulence intensity I_u.

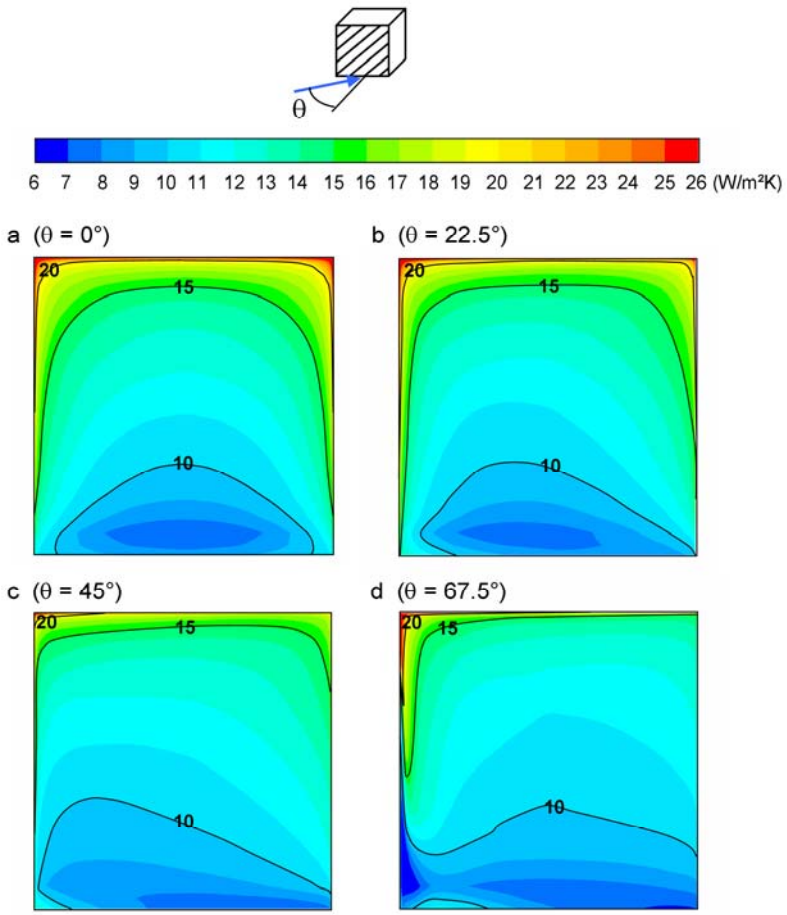

Figure 8. Distribution of CHTC across the windward facade, for U_{10} = 3 m/s and for wind directions θ = 0, 22.5, 45 and 67.5°.

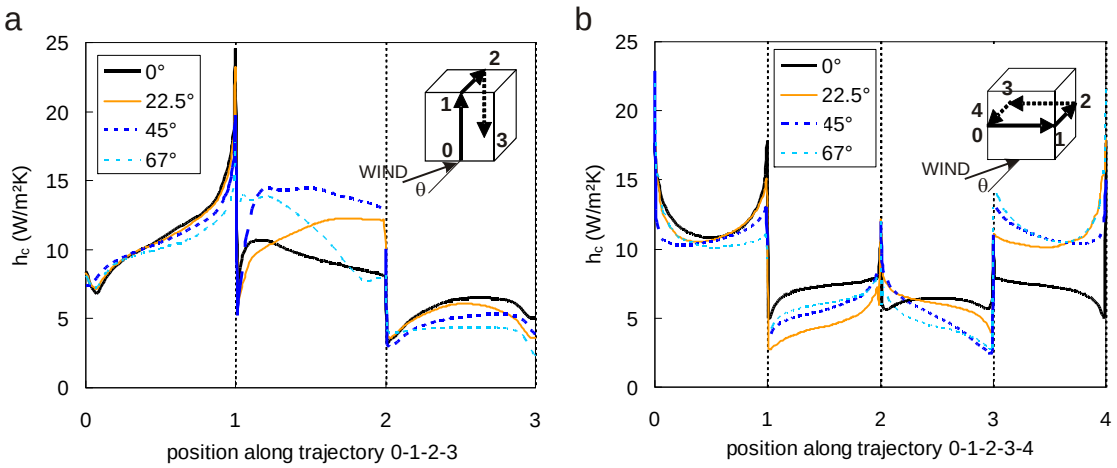

Figure 9. CHTC along lines on the building surface, for U_{10} = 3 m/s and for wind directions θ = 0, 22.5, 45 and 67.5°.

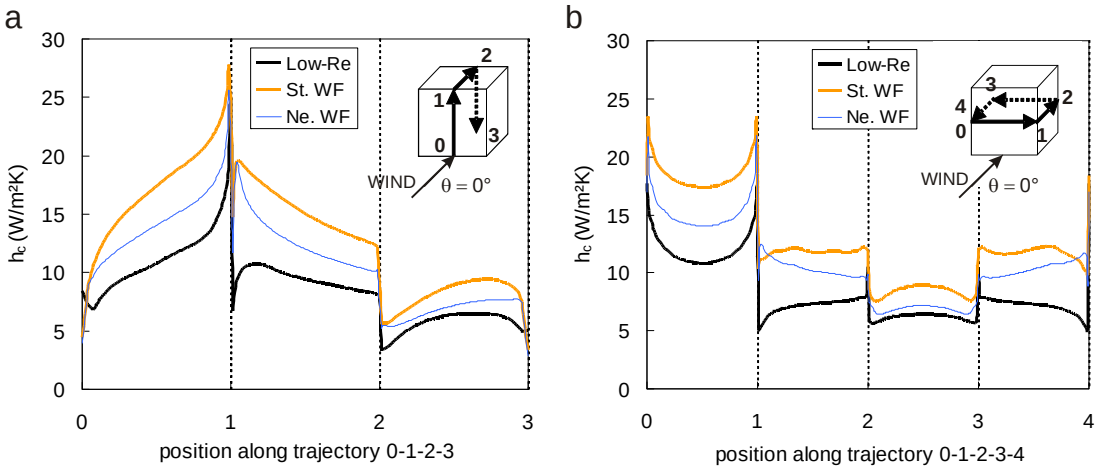

Figure 10. Comparison between CHTC obtained by low-Reynolds number modelling (low-Re), standard wall functions (St. WF) and non-equilibrium wall functions (Ne. WF). Results are presented along lines on the building surface, for U_{10} = 3 m/s and θ = 0°.

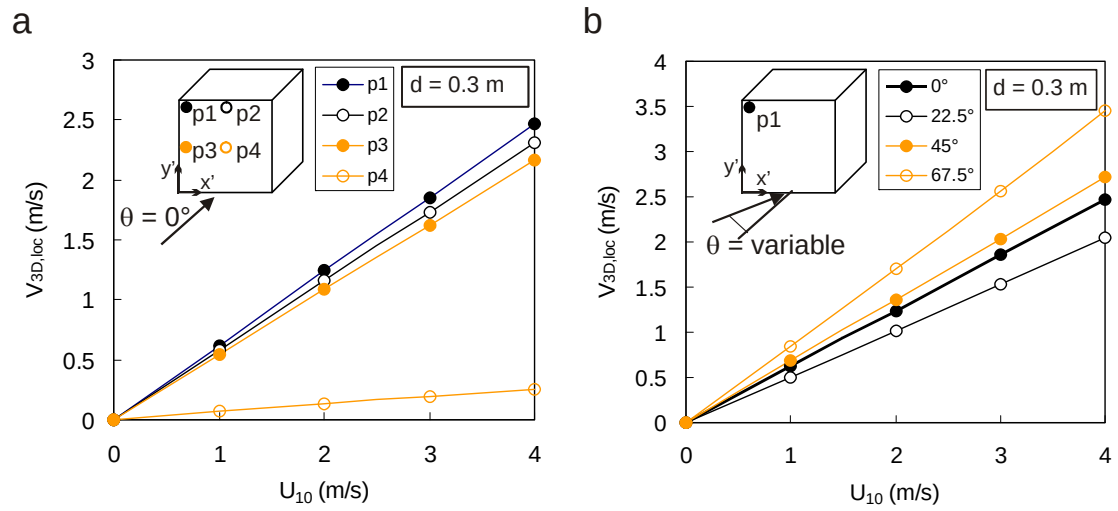

Figure 11. $V_{3D,loc}$ at 0.3 m from the facade as a function of U_{10}. (a) At four different points at the windward facade and for θ = 0°. (b) At point p1 and for θ = 0, 22.5, 45 and 67.5°.

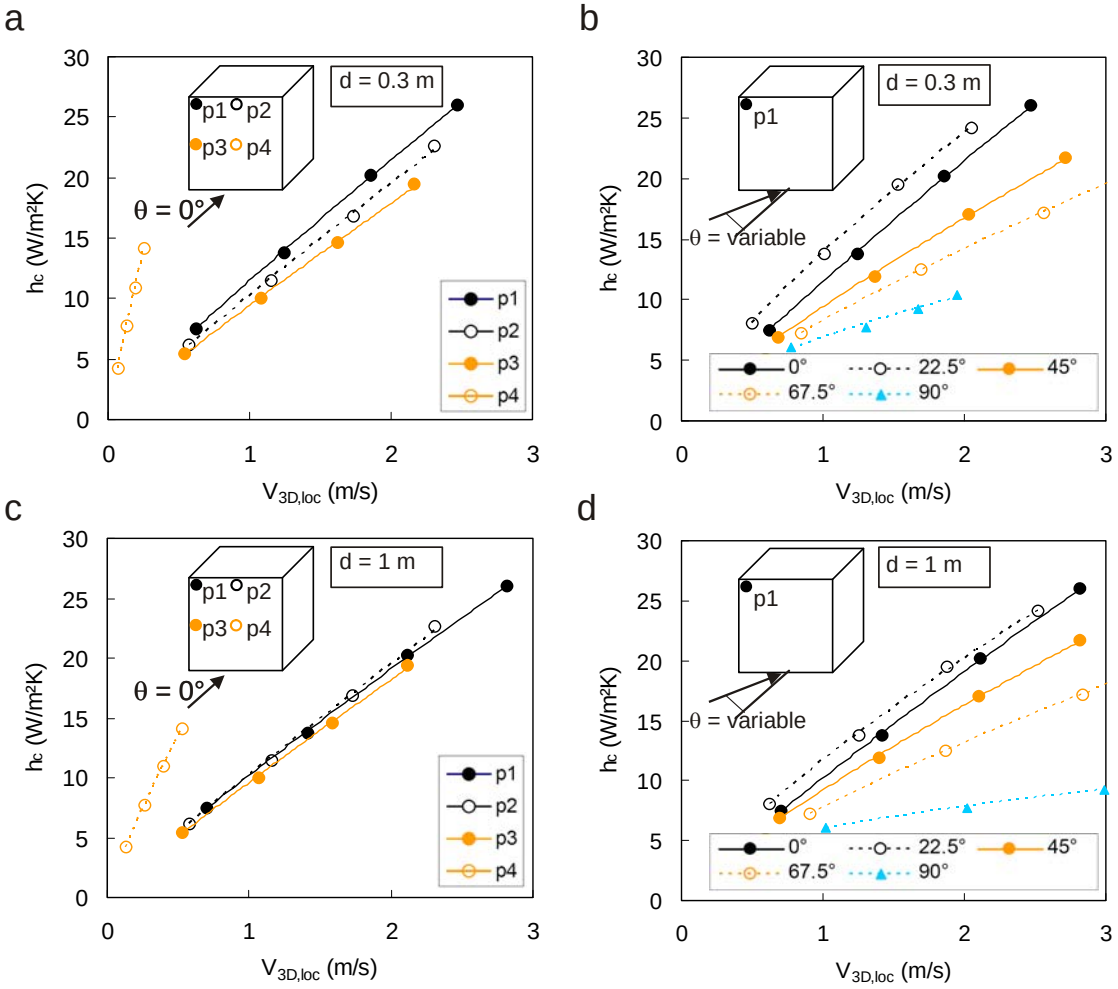

Figure 12. CHTC as a function of $V_{3D,loc}$, for (a) four points at the facade, d = 0.3 m and θ = 0°; (b) point p1, d = 0.3 m and θ = 0, 22.5, 45, 67.5 and 90°; (c) same as (a) but for d = 1 m; (d) same as b but for d = 1 m.

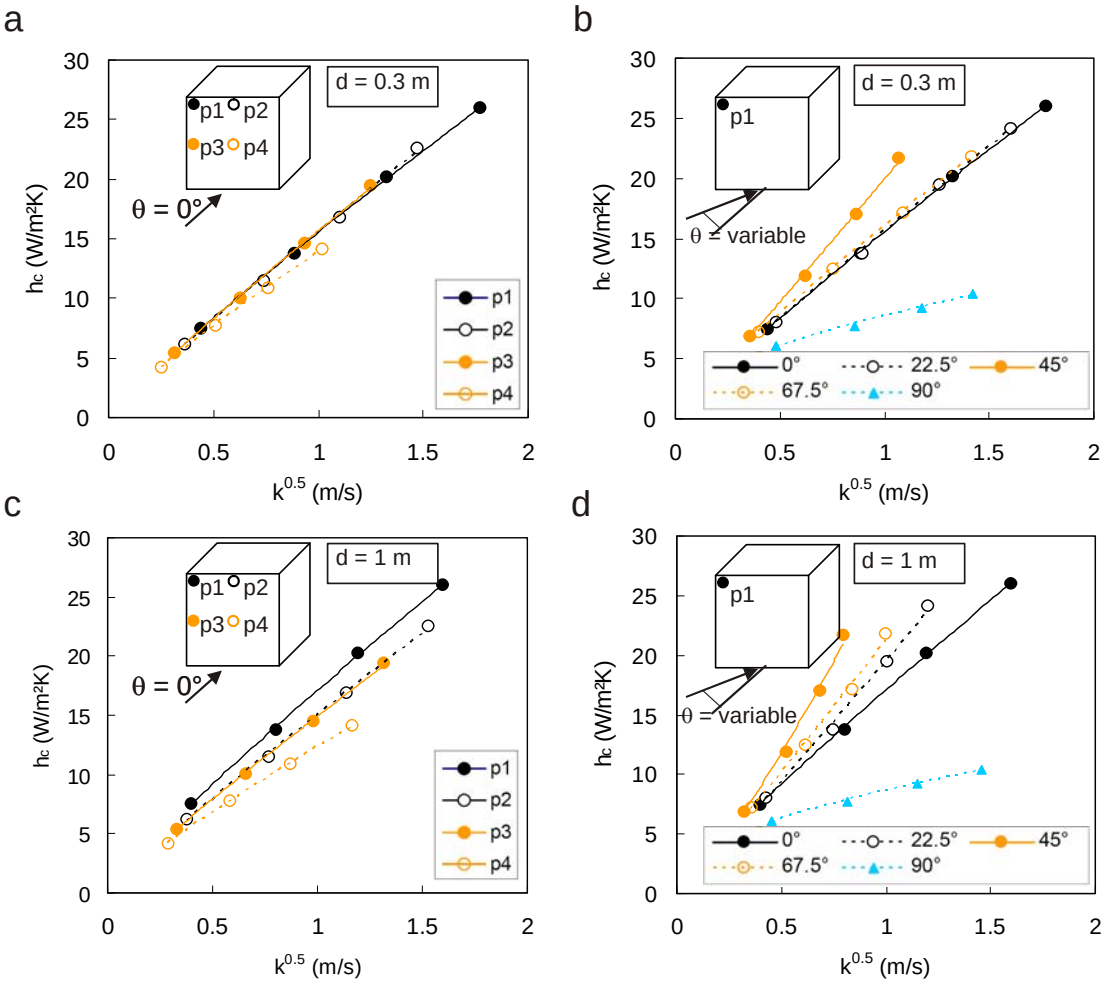

Figure 13. CHTC as a function of $k^{0.5}$, for (a) four points at the facade, d = 0.3 m and θ = 0°; (b) point p1, d = 0.3 m and θ = 0, 22.5, 45, 67.5 and 90°; (c) same as (a) but for d = 1 m; (d) same as b but for d = 1 m.

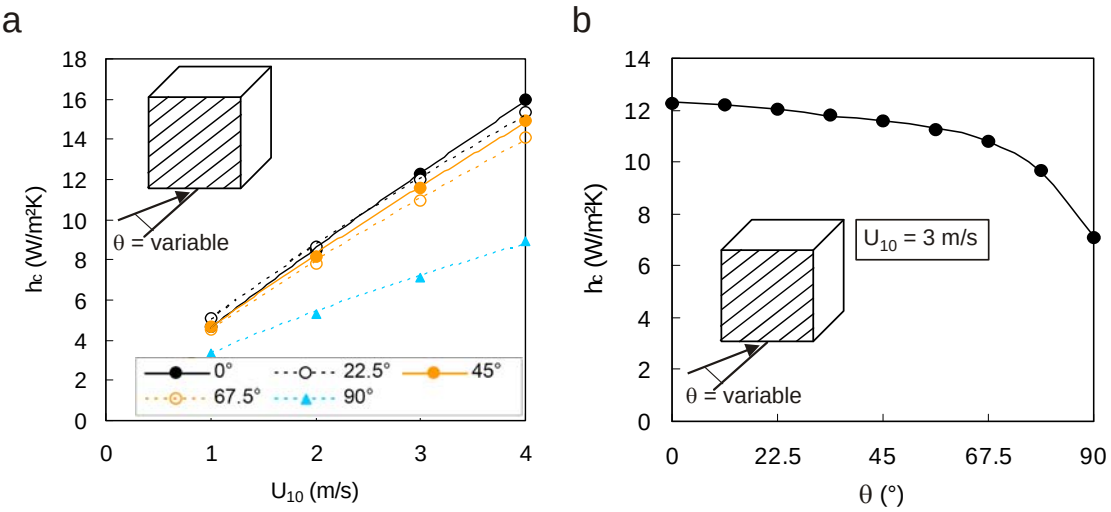

Figure 14. (a) Surface-averaged CHTC as a function of U_{10}, with θ as a parameter; and (b) surface-averaged CHTC as a function of θ, for U_{10} = 3 m/s.

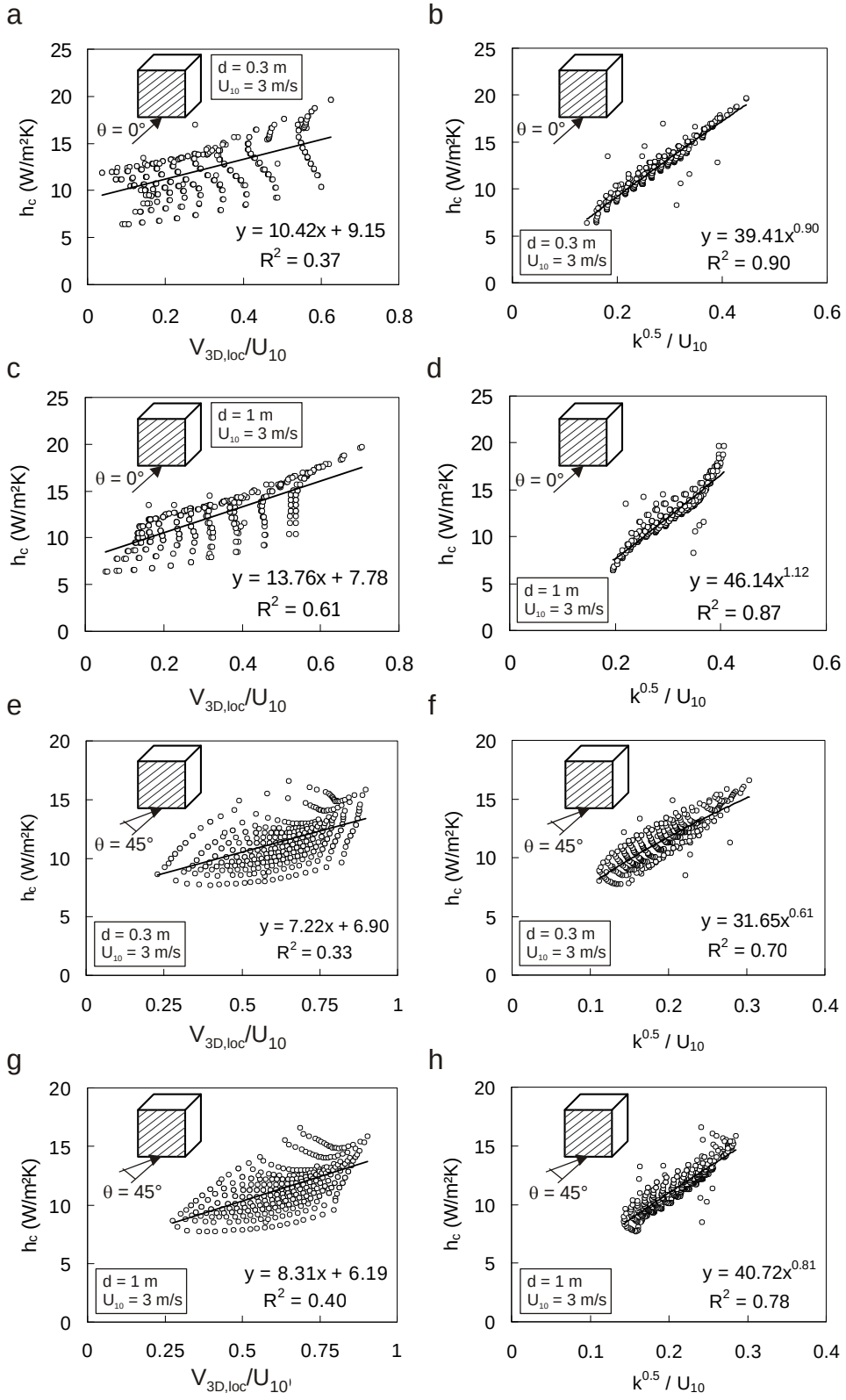

Figure 15. Correlations across the facade of the local CHTC with the local ratio $V_{3D,loc}/U_{10}$ (a,c,e,g) and with the local ratio $k^{0.5}/U_{10}$ (b,d,f,h), for U_{10} = 3 m/s and for different combinations of the parameters θ and d.

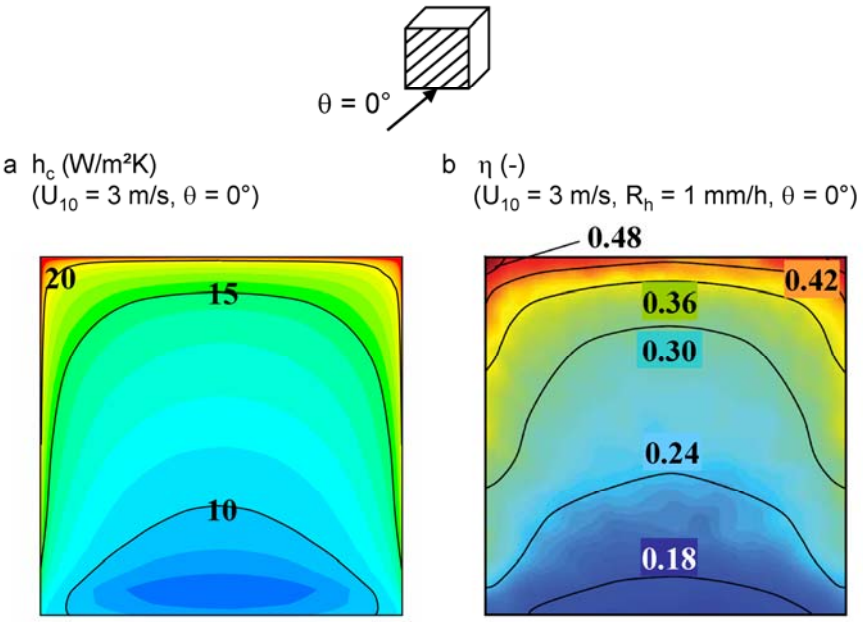

Figure 16. Distribution of CHTC across the windward facade, for U_{10} = 3 m/s, θ = 0°; (b) Distribution of the WDR catch ratio η across the same windward facade, for U_{10} = 3 m/s, R_h = 1 mm/h, θ = 0°.

Table 1. Parameters in the two logarithmic law fits through the experimental mean wind speed data.

	Log-law 1	Log-law 2
U_H (m/s)	1	1
z_0 (m)	7.3E-07	0.0015
u^*_{ABL} (m/s)	0.034	0.086
κ (-)	0.42	0.42

Table 2. Correlations between CHTC and local wind speed $V_{3D,loc}$, for wind direction 0°, at different positions at the windward facade (p1-p4) and at a distance d = 0.3 m and 1 m from the facade.

Wind direction (°)	Position (-)	Distance (m)	Regression equation (-)	R^2 (-)
0	p1	0.3	$h_c = 11.5V_{3D,loc}^{0.90}$	0.9996
0	p2	0.3	$h_c = 10.2V_{3D,loc}^{0.93}$	0.9991
0	p3	0.3	$h_c = 9.4V_{3D,loc}^{0.92}$	0.9994
0	p4	0.3	$h_c = 50.1V_{3D,loc}^{0.92}$	0.9996
0	p1	1	$h_c = 10.2V_{3D,loc}^{0.90}$	0.9996
0	p2	1	$h_c = 10.2V_{3D,loc}^{0.93}$	0.9991
0	p3	1	$h_c = 9.6V_{3D,loc}^{0.92}$	0.9994
0	p4	1	$h_c = 24.6V_{3D,loc}^{0.87}$	0.9990

Table 3. Correlations between CHTC and local wind speed $V_{3D,loc}$ at position p1 at the windward facade, for different wind directions and at a distance d = 0.3 m and 1 m from the facade.

Wind direction (°)	Position (-)	Distance (m)	Regression equation (-)	R^2 (-)
0	p1	0.3	$h_c = 11.5V_{3D,loc}^{0.90}$	0.9996
22.5	p1	0.3	$h_c = 13.8V_{3D,loc}^{0.78}$	0.9996
45	p1	0.3	$h_c = 9.4V_{3D,loc}^{0.83}$	0.9989
67.5	p1	0.3	$h_c = 8.2V_{3D,loc}^{0.79}$	1.0000
0	p1	1	$h_c = 10.2V_{3D,loc}^{0.90}$	0.9996
22.5	p1	1	$h_c = 11.7V_{3D,loc}^{0.79}$	0.9996
45	p1	1	$h_c = 9.2V_{3D,loc}^{0.82}$	0.9991
67.5	p1	1	$h_c = 7.7V_{3D,loc}^{0.77}$	1.0000

Table 4. Correlations between CHTC and turbulent kinetic energy k, for wind direction 0°, at different positions at the windward facade (p1-p4) and at a distance d = 0.3 m and 1 m from the facade.

Wind direction (°)	Position (-)	Distance (m)	Regression equation (-)	R^2 (-)
0	p1	0.3	$h_c = 15.6k^{0.45}$	0.9996
0	p2	0.3	$h_c = 15.6k^{0.46}$	0.9991
0	p3	0.3	$h_c = 15.7k^{0.45}$	0.9994
0	p4	0.3	$h_c = 13.9k^{0.43}$	1.0000
0	p1	1	$h_c = 17.1k^{0.45}$	0.9995
0	p2	1	$h_c = 15.0k^{0.46}$	0.9991
0	p3	1	$h_c = 14.9k^{0.45}$	0.9994
0	p4	1	$h_c = 12.3k^{0.43}$	1.0000

Table 5. Correlations between CHTC and turbulent kinetic energy k, at position p1 at the windward facade, for different wind directions and at a distance d = 0.3 m and 1 m from the facade.

Wind direction (°)	Position (-)	Distance (m)	Regression equation (-)	R^2 (-)
0	p1	0.3	$h_c = 15.6k^{0.45}$	0.9996
22.5	p1	0.3	$h_c = 15.6k^{0.46}$	0.9995
45	p1	0.3	$h_c = 20.0k^{0.52}$	0.9983
67.5	p1	0.3	$h_c = 16.1k^{0.43}$	0.9998
0	p1	1	$h_c = 17.1k^{0.45}$	0.9995
22.5	p1	1	$h_c = 19.5k^{0.53}$	0.9972
45	p1	1	$h_c = 27.8k^{0.61}$	0.9947
67.5	p1	1	$h_c = 21.3k^{0.53}$	0.9974

Table 6. Correlations between surface-averaged CHTC for the windward facade and reference wind speed U_{10}.

Wind direction (°)	Position (-)	Regression equation (-)	R^2 (-)
0	windward	$h_c = 4.6U_{10}^{0.89}$	0.9999
22.5	windward	$h_c = 5.0U_{10}^{0.80}$	0.9995
45	windward	$h_c = 4.6U_{10}^{0.84}$	0.9996
67.5	windward	$h_c = 4.5U_{10}^{0.81}$	0.9996

Table 7. Variation of surface-averaged CHTC as a function of the maximum value of the incident longitudinal turbulence intensity, $I_{u,max}$.

$I_{u,max}$ (%)	h_c (W/m²K)	h_c increase (%)
1.5	7.4	0
6.7	11.0	49
10.5	12.3	66
13.6	13.2	79
15.4	14.0	89